PHYSICAL REVIEW B **86**, 060407(R) (2012)

Investigation of the spin exchange interactions and the magnetic structure of the high-temperature multiferroic $CuBr_2$

C. Lee,[1] Jia Liu,[1] M.-H. Whangbo,[1] H.-J. Koo,[2] R. K. Kremer,[3,*] and A. Simon[3]

[1]*Department of Chemistry, North Carolina State University, Raleigh, North Carolina 27695-8204, USA*

[2]*Department of Chemistry and Research Institute of Basic Science, Kyung Hee University, Seoul 130-701, Republic of Korea*

[3]*Max Planck Institut für Festkörperforschung, Heisenbergstrasse 1, D-70569 Stuttgart, Germany*

(Received 24 March 2012; revised manuscript received 18 July 2012; published 21 August 2012)

We report a detailed density functional analysis of the spin exchange interactions and the magnetic structure of the high-temperature multiferroic $CuBr_2$ and compare the results with magnetic susceptibility measurements. $CuBr_2$ shows one-dimensional antiferromagnetism and undergoes long-range antiferromagnetic ordering at ∼74 K. Due to the competition between the nearest- and next-nearest-neighbor spin exchanges, each Cu^{2+} chain has a cycloidal spin-spiral structure, which is described approximately by a quadrupling of the nuclear cell with spin moment rotation of ∼85° in the plane of the $CuBr_2$ ribbon plane.

DOI: 10.1103/PhysRevB.86.060407 PACS number(s): 75.40.Cx, 75.30.Et, 77.84.−s, 75.40.−s

The quest for high performance multiferroic materials is stimulated by the expectation to control magnetic properties by electric fields and, vice versa, electric polarization by magnetic fields. Multiferroics may open routes to tunable magneto-optical/magnetoelectric multifunctional memory devices. (For recent reviews on multiferroics, see Refs. 1–5.) Well-known multiferroics are mostly oxides of transition metals with open *d* shells; systems with other anions have less intensively been investigated. In a large number of multiferroics the ferroelectricity is induced by spiral magnetic ordering that removes inversion symmetry.[6–8] Spiral magnetic order is often realized in a magnetic chain system with competing nearest-neighbor (NN) and next-nearest-neighbor (NNN) spin exchange interactions, and often gives rise to an incommensurate long-range ordered antiferromagnetic (AFM) cycloidal magnetic structures.[9–11] Such a spiral magnetic order removes inversion symmetry so that, with the resulting noncentrosymmetric spin structure, spin-orbit interaction gives rise to asymmetric charge distribution, thereby inducing a permanent dielectric polarization and ferroelectricity below the Néel temperature T_N.[12,13] Multiferroicity has been found in spiral quantum chain systems such as $LiCu_2O_2$ and $LiCuVO_4$,[14,15] which consist of CuO_2 ribbon chains that are made up of edge-sharing CuO_4 squares. In $LiCuVO_4$, for example, the NN spin exchange (i.e., the Cu-O-Cu superexchange) is ferromagnetic (FM) while the NNN spin exchange (i.e., the Cu-O···O-Cu spin exchange) via oxygen anions is AFM exchange.[10,12,16] Our notion that the magnitude of the NNN is about three times greater than the NN spin exchange[10,12,16,17] has recently been questioned.[18] The possibility of favorably switching the ferroelectric polarization of $LiCuVO_4$ with external electric and magnetic fields has been demonstrated by polarized neutron diffraction experiments by Mourigal *et al.*[19]

Recently, we have shown that anhydrous $CuCl_2$, which crystallizes with a structure containing $CuCl_2$ ribbon chains similar to the aforementioned oxocuprates, also shows a spiral-magnetic ordering below a Néel temperature of ∼23 K.[20] Subsequently, Seki *et al.* have observed multiferroicity in $CuCl_2$.[21] Until recently, the magnetic properties of the structurally very similar $CuBr_2$ (Ref. 22) have remained largely unknown. A measurement of the magnetic susceptibility by Barraclough and Ng revealed a broad maximum at 225 K, indicating low-dimensional AFM short-range ordering but no evidence for long-range AFM ordering was found.[23] Subsequent heat capacity and nuclear-quadrupole-resonance (NQR) studies proved long-range AFM ordering below 74 K.[24,25] Recently, Zhao *et al.* have found multiferroicity in $CuBr_2$ below its Néel temperature and shown that the AFM ground state is an incommensurate spin spiral propagating along the ribbon chains with the spiral plane within the plane of the $CuBr_2$ ribbon chains.[26] In the following we investigate the magnetic properties of $CuBr_2$ on the basis of density functional theory (DFT) calculations by evaluating the spin exchange constants and the magnetic anisotropy energy for a single Cu^{2+} ion, and compare the theoretical results with the magnetic structure and the exchange constants deduced from the fitting analysis of the magnetic susceptibility data of $CuBr_2$.

Theory: Evaluation of spin exchange constants. In view of bond distances and angles of the crystal structure [Fig. 1(a)], we consider a set of five spin exchange paths, $J_1, \ldots, J_5$ [Fig. 1(b)], in $CuBr_2$. Here J_1 and J_2 are the intrachain NN and NNN exchanges, J_{NN} and J_{NNN}, respectively, while J_3, J_4, and J_5 are interchain spin exchanges. To determine these spin exchange parameters, we perform energy-mapping analysis[27] based on DFT calculations by calculating the relative energies of the six ordered spin states (FM and AF1–AF5) of $CuBr_2$ depicted in Fig. 1(c). Our calculations employed the frozen-core projector augmented wave method[28,29] encoded in the Vienna *ab initio* simulation package[30] with the generalized-gradient approximation (GGA),[31] the plane-wave cutoff energy of 330 eV, and 36 *k* points for the irreducible Brillouin zone. To properly describe the strong electron correlation associated with Cu 3*d* states, the DFT plus on-site repulsion U (DFT + U) method of Dudarev *et al.*[32] was employed with effective $U_{eff} = U - J = 3$, 5, and 7 eV on Cu atoms. In the DFT + U method of Liechtenstein *et al.*[33] the energy formula includes the on-site repulsion U and the exchange correction J separately, whereas in the DFT + U method of Dudarev *et al.* the energy formula includes only the difference $U_{eff} = U - J$. It has been pointed out[34] that spin canting and magnetocrystalline anisotropy depend strongly on J. Thus, in determining the magnetocrystalline anisotropy energy of

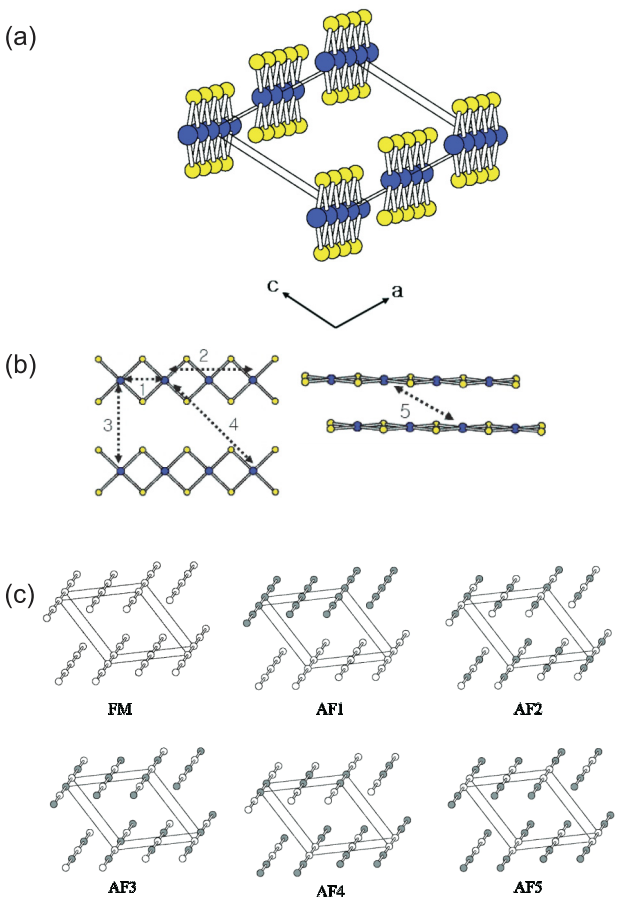

FIG. 1. (Color online) (a) Crystal structure of $CuBr_2$ with Cu-Br bonds highlighted. The Cu and Br atoms are represented by blue and yellow circles, respectively. The b axis is along the $CuBr_2$ ribbon chain, and is perpendicular to the ac plane. (b) Three-dimensional arrangements of the spin exchange paths J_1, J_2, J_3, J_4, and J_5 in $CuBr_2$. (c) Ordered spin arrangements of $CuBr_2$ employed to extract the spin exchange constants by energy-mapping analysis. The up spins and down spins at the copper sites are represented by the empty and solid circles, respectively.

the Cu^{2+} ions, we carried out DFT + U calculations including spin-orbit coupling (SOC) by employing the DFT + U method of Dudarev *et al.*[32] and that of Liechtenstein *et al.*[33] with $J = 1$ eV.

In terms of the spin Hamiltonian,

$$H = -\sum_{i,j} J_{ij} \vec{S}_i \vec{S}_j, \tag{1}$$

where J_{ij} ($=J_1$–J_5) are the exchange parameters between the unpaired spin sites i and j, the total spin exchange interaction energies (per formula unit) of the six ordered spin states are expressed as

$$E_{FM} = (-2J_1 - 2J_2 - 2J_3 - 4J_4 - 4J_5)\frac{N^2}{4}, \tag{2}$$

$$E_{AF1} = (-2J_1 - 2J_2 + 2J_3 + 4J_4 + 4J_5)\frac{N^2}{4}, \tag{3}$$

$$E_{AF2} = (+2J_1 - 2J_2 - 2J_3 - 4J_4 + 4J_5)\frac{N^2}{4}, \tag{4}$$

TABLE I. Spin exchange parameters J_{NN}, J_{NNN}, J_3, J_4, and J_5 (in K) of $CuBr_2$ obtained from GGA + U calculations with $U_{eff} = 3$, 5, and 7 eV. The rightmost column contains the spin exchange parameters of $CuCl_2$ for $U_{eff} = 7$ eV for comparison (Ref. 20).

J_i $U_{eff} =$	3 eV	5 eV	7 eV	7 eV ($CuCl_2$)
$J_1 \equiv J_{NN}$	227	231.3	231	213.5
$J_2 \equiv J_{NNN}$	− 829	− 698.1	− 593	− 284.3
J_3	− 289.4	− 250.1	− 212.7	− 61.5
J_4	− 3.0	− 5.6	− 4.0	− 1.2
J_5	− 28.9	− 29.4	− 25.6	− 5.8
J_{NN}/J_{NNN}	− 0.27	− 0.33	− 0.39	− 0.75

$$E_{AF3} = (+2J_1 - 2J_2 + 2J_3 + 4J_4 - 4J_5)\frac{N^2}{4}, \tag{5}$$

$$E_{AF4} = (+2J_2 - 2J_3 + 4J_4)\frac{N^2}{4}, \tag{6}$$

$$E_{AF5} = (+2J_2 + 2J_3 - 4J_4)\frac{N^2}{4}, \tag{7}$$

where N is the number of unpaired spins at each spin site (i.e., $N = 1$ in the present case). Thus, we obtain the values of J_1–J_5 summarized in Table I by mapping the relative energies of the six ordered spin states determined from the GGA + U calculations onto the corresponding relative energies from the total spin exchange energies.[27,35]

Table I shows that the dominating exchange parameters are the intrachain NN and NNN exchanges, where J_{NN} is FM and J_{NNN} is AFM, the latter being larger than J_{NN} by a factor of 3. The strongest interchain spin exchange J_3 couples the Cu spin moments along [1,0,1] via Cu-Br$\cdots$Br-Cu super-superexchange paths. J_3 is weaker than J_{NNN} by a factor of 3 and consequently $CuBr_2$ must be considered as a quasi-two-dimensional spin system with important implications for the pitch angle and the description of the magnetic susceptibility (see below).[36,37] J_4 and J_5 are negligibly small compared with J_1, J_2, and J_3.

Theory: Spin spiral state. To gain insight into the spin spiral state of $CuBr_2$, we performed a series of calculations for the spin spiral state with propagation vector $q = (0,q_y,0.5)$ as a function of q_y using the plane-wave cutoff energy of 400 eV and a set of 96 k points in the irreducible Brillouin zone. The dependence of the electronic energy $E(q)$ on q_y is presented in Fig. 2, which shows that the energy at $q_y = 0$ (i.e., the FM arrangement between all NN Cu spin moments) is lower than that at $q_y = 0.5$ (i.e., a AFM arrangement between all NN Cu spin moments). The energy minimum occurs at around $q_y \sim 0.22$ in all GGA + U calculations with different U_{eff} values, which is close to the y component of the propagation vector describing the magnetic structure of $CuBr_2$ (see below).

Theory: Magnetic anisotropy energy. We determine the magnetic anisotropy energy of the Cu^{2+} ions of $CuBr_2$ by performing GGA + U + SOC calculations on the ferromagnetic state of $CuBr_2$ with a set of 96 k points in the irreducible Brillouin zone and a plane-wave cutoff energy of 400 eV. Since SOC is a local interaction associated with a given magnetic ion, this approximation is justified. In good agreement with the result of the magnetic structure determination (see below),

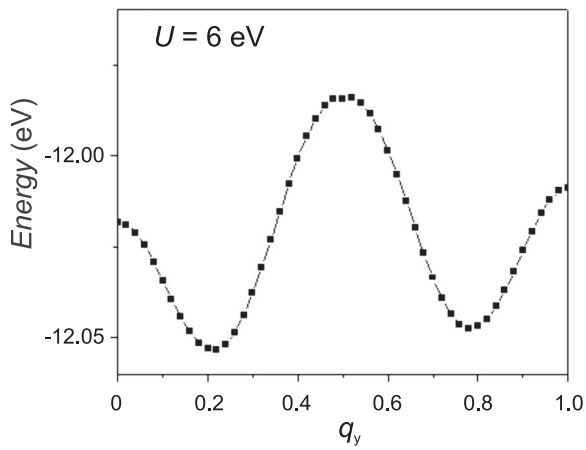

FIG. 2. Total energy $E(q)$ calculated for the spin spiral state of $CuBr_2$ as a function of $q = (0,q_y,0.5)$ on the basis of the noncollinear DFT + U (with $U_{\rm eff} = 6$ eV) method using a unit cell containing two formula units.

our GGA + U + SOC calculations with $U_{\rm eff} = 3$, 5, and 7 eV show that spin orientations lying in the $CuBr_4$ square planes, i.e., ≈(1,0,1), containing the x^2-y^2 magnetic orbital, are more stable than the spin orientation perpendicular to the $CuBr_2$ ribbon planes by 0.25, 0.22, and 0.16 meV/Cu, respectively, from the DFT + U method of Liechtenstein *et al.*, and by 0.28, 0.20, and 0.15 meV/Cu, respectively, from the DFT + U method of Dudarev *et al.*. Namely, the Cu^{2+} ions of $CuBr_2$ have easy-plane anisotropy, as has similarly been found for $CuCl_2$ and $LiCuVO_4$.[9,16,20]

Experiment. Free-standing black crystalline platelets up to a length of approximately 1 cm of $CuBr_2$ were grown from a concentrated solution of CuO in HBr.[22,38] The soft and very pliable crystals cleave readily in the *ab* plane. Crystalline pieces were carefully cut and temperature and field dependent magnetic susceptibilities were measured with fields within the *ab* plane by using a superconducting quantum interference device magnetometer (MPMS7, Quantum Design, 6325 Lusk Boulevard, San Diego, CA.). Figure 3 shows the magnetic susceptibility of $CuBr_2$. Long-range AFM ordering below a Néel temperature $T_N = 73.2(5)$ K is clearly evidenced by the kink in the magnetic susceptibility.[25,26] As observed early on by Barraclough and Ng, and recently substantiated by Zhao *et al.*, substantial AFM short-range ordering is visible far above T_N indicated by a very broad maximum in the susceptibility at around 225(10) K.[23,26] In Fig. 3 we compare the results of density-matrix renormalization group (DMRG) calculations of the magnetic susceptibility of a frustrated chain with competing FM NN and AFM NNN interactions, i.e., $J_{\rm NN} > 0$ and $J_{\rm NNN} < 0$, with our experimental data, which have been corrected for diamagnetic and van Vleck contributions, and a small Curie contribution of 0.25% associated with free $S = 1/2$ entities.[20] In order to take into consideration the interchain spin exchange coupling we applied a mean-field correction to the DMRG susceptibility calculations $\chi_{\rm spin}$ according to[39]

$$\chi_{\rm spin}^{\rm cor}(T) = \frac{\chi_{\rm spin}(T)}{1 - \left(zJ_3/N_{\rm A}g^2\mu_{\rm B}^2\right)\chi_{\rm spin}(T)}, \qquad (8)$$

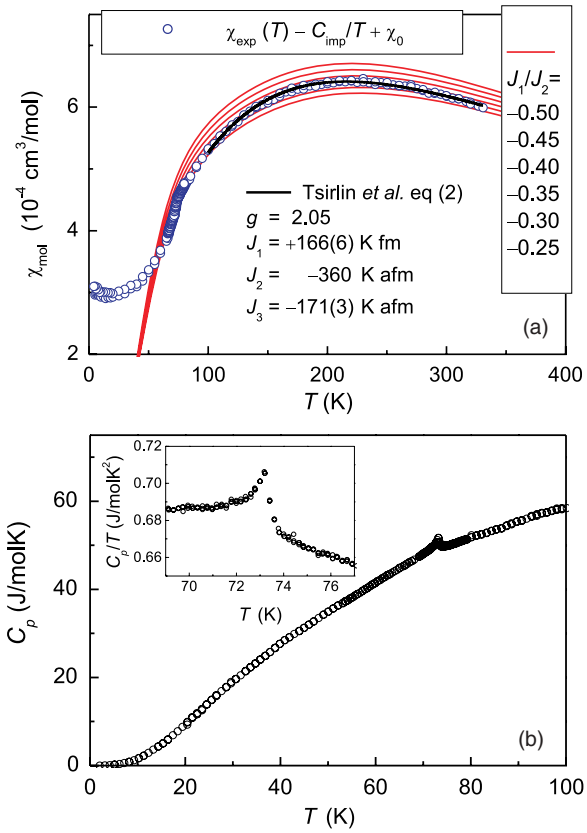

FIG. 3. (Color online) (a) Magnetic susceptibility $\chi_{\rm mol}$ of $CuBr_2$ measured parallel to the crystal platelets corrected by a temperature independent χ_0, i.e., the sum of the diamagnetic contribution of the closed shells and paramagnetic van Vleck contributions ($+41 \times 10^{-6}$ cm^3/mol) and a Curie-like contribution, C/T, with the Curie constant C corresponding to 0.25% $S = 1/2$ spin entities. A kink at 74(1) K due to AFM ordering is clearly visible. The theoretical susceptibilities of a frustrated $J_{\rm NN}$-$J_{\rm NNN}$ chain with ratios $J_{\rm NN}/J_{\rm NN}$ (from top to bottom), g factor, and J_2 ($=J_{\rm NNN}$) = 360 K, as indicated in the inset are given by the (red) solid lines with ratios of $J_{\rm NN}/J_{\rm NNN}$ as indicated (Refs. 40 and 41). The (black) solid line is a fit of a high-temperature series expansion of the susceptibility according Eq. (2) in Ref. 37 with parameters listed in the upper inset. (b) Heat capacity of $CuBr_2$. The inset displays the λ-type anomaly in the heat capacity near the Néel temperature (Ref. 26).

where $N_{\rm A}$ is Avogadro's number, $\mu_{\rm B}$ is the Bohr magneton, and g is the g factor.

Good agreement between experiment and theory is found for the ratios $-0.40 < J_1/J_2 < -0.30$ assuming $J_2 = J_{\rm NNN}$ as the only adjustable parameter, with $J_{\rm NNN} = -360$ K and a value for the interchain coupling J_3 of ∼−130 K implied by the ratio $J_3/J_{\rm NNN} \approx 0.35$ found in the DFT calculations.[40,41] The ratio of $J_{\rm NN}$ to $J_{\rm NNN}$ is in very good accordance with the results of the DFT calculations (see Table I). However, the strengths of $J_{\rm NN}$ and $J_{\rm NNN}$ are overestimated by a factor of ∼2, as is typically found for DFT + U calculations.[27,42]

Tsirlin *et al.* have proposed a high-temperature series expansion (HTSE) up to third order in temperature for the susceptibility of a chain with NN and NNN and interchain

spin exchange coupling J_3 according to[37]

$$\chi(T)^{\mathrm{HTSE}} = \frac{N_A g^2 \mu_B^2}{4k_B T}\left(1 + \frac{J_{\mathrm{NN}} + J_{\mathrm{NNN}} + J_3}{2T} + \frac{J_{\mathrm{NN}}^2 + J_{\mathrm{NNN}}^2 + J_3^2}{4T^2}\right)^{-1}. \quad (9)$$

The experimental data were fitted to Eq. (9) by assuming $J_{\mathrm{NNN}} = -360$ K and varying J_{NN} and J_3. The best fit given as a (black) solid line in Fig. 3 reproduces well the experimental data for $T \geqslant 100$ K. The fitted values of J_{NN} and J_3 are equal in magnitude, consistent with the findings of the DFT calculations.

As already briefly summarized by Zhao *et al.*, neutron powder diffraction patterns collected at ILL's medium resolution high-intensity powder diffractometer[43] D20 ($\lambda = 2.40$ Å) upon cooling below ~74 K showed additional magnetic Bragg reflections, which can be indexed using a propagation vector [1,0.2350(3),0.5]. A symmetry analysis using the program BASIREPS[44] with Cu at the Wyckoff position $2a$ (0,0,0) in the space group $C2/m$ gave one irreducible representation of dimension one. The profile refinement of the magnetic structure was successfully performed on difference patterns, i.e., subtracting the nuclear scattering represented by the 80 K diffraction pattern. The latter was separately refined in order to fix the scale factor for the refinement of the magnetic moment. The magnetic structure of $CuBr_2$ is shown in Fig. 4. The total moment was refined to $0.38(2)\mu_B$ with components $m_x = 0.28(4)\mu_B$, $m_z = 0.41(3)\mu_B$, $-im_y = 0.39(2)\mu_B$, and all other components zero, within error bars, implying a cycloidal spin helix propagating along the crystallographic b axis. Accordingly, the plane of the spin helix is slightly inclined [~13(2)°] away from the $CuBr_2$ ribbon planes. The Cu^{2+} spin moment $0.38\mu_B$ is significantly reduced from $1\mu_B$ due to quantum effects, but close to what has been found, e.g., in $LiCuVO_4$, $CuCl_2$, and $NaCu_2O_2$ ($0.31\mu_B$, $0.5\mu_B$, and $0.54\mu_B$), respectively.[9,20,45] Both $CuCl_2$ and $CuBr_2$ systems are NN/NNN chain systems. The DFT result for $CuCl_2$ points to a larger ratio of $J_{\mathrm{NN}}/J_{\mathrm{NNN}}$ than for $CuBr_2$. However, this was not observed experimentally. According to the experiments the ratio $J_{\mathrm{NN}}/J_{\mathrm{NNN}}$ is almost identical.[20] The leading interchain spin exchange J_3/J_{NNN} in $CuBr_2$ is significantly larger than in $CuCl_2$ (0.36 versus 0.22), indicating that $CuBr_2$ has more of a quasi-two-dimensional character than $CuCl_2$. We attribute this trend to the larger extension of the Br $4p$ wave functions. Neither a change of the space group symmetry nor noticeable variations of the Br atom positions could be detected on passing the Néel temperature.

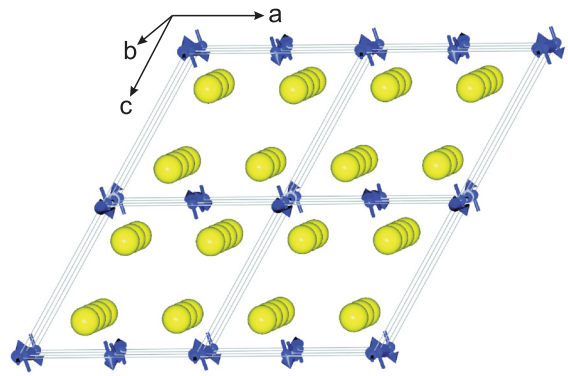

FIG. 4. (Color online) Magnetic structure of $CuBr_2$ at 1.65 K. The Cu and Br atoms are represented by blue and yellow circles, respectively.

In conclusion, the magnetic properties of $CuBr_2$ are dominated by the intrachain FM exchange J_{NN}, the intrachain AFM exchange J_{NNN}, and the interchain AFM exchange J_3. Our noncollinear spin structure calculations show the (1,0.24,0.5) magnetic superstructure due to the intrachain spin frustration associated with J_{NN} and J_{NNN}. This, combined with the in-plane anisotropy of the Cu^{2+} ion, predicts a cycloidal spin-spiral structure for $CuBr_2$, which approximately quadruples the chemical unit cell with spin moment rotation in the plane of the $CuBr_2$ ribbon plane. This prediction is in excellent agreement with experiment.

The authors would like to thank E. Brücher and G. Siegle for experimental assistance. Work at NCSU was supported by the computing resources of the NERSC center and the HPC center of NCSU.

*Corresponding author: r.kremer@fkf.mpg.de

[1] N. A. Spaldin and M. Fiebig, Science **309**, 391 (2005).
[2] M. Fiebig, J. Phys. D: Appl. Phys. **38**, R123 (2005).
[3] D. I. Khomskii, J. Magn. Magn. Mater. **306**, 1 (2006).
[4] S. W. Cheong and M. Mostovoy, Nat. Mater. **6**, 13 (2007).
[5] Y. Tokura, J. Magn. Magn. Mater. **310**, 1145 (2007).
[6] T. Kimura, T. Goto, H. Shintani, K. Ishizaka, T. Arima, and Y. Tokura, Nature (London) **426**, 55 (2003).
[7] M. Mostovoy, Phys. Rev. Lett. **96**, 067601 (2006).
[8] T. Kimura, Annu. Rev. Mater. Res. **37**, 387 (2007).
[9] B. J. Gibson, R. K. Kremer, A. V. Prokofiev, W. Assmus, and G. J. McIntyre, Physica B **350**, E253 (2004).
[10] M. Enderle, C. Mukherjee, B. Fåk, R. K. Kremer, J.-M. Broto, H. Rosner, S.-L. Drechsler, J. Richter, J. Malek, A. Prokofiev, W. Assmus, S. Pujol, J.-L. Raggazzoni, H. Rakoto, M. Rheinstädter, and H. M. Rønnow, Europhys. Lett. **70**, 237 (2005).
[11] L. Capogna, M. Mayr, P. Horsch, M. Raichle, R. K. Kremer, M. Sofin, A. Maljuk, M. Jansen, and B. Keimer, Phys. Rev. B **71**, 140402(R) (2005).
[12] H. J. Xiang and M.-H. Whangbo, Phys. Rev. Lett. **99**, 257203 (2007).
[13] H. J. Xiang, S.-H. Wei, M.-H. Whangbo, and J. L. F. Da Silva, Phys. Rev. Lett. **101**, 037209 (2008).
[14] S. Park, Y. J. Choi, C. L. Zhang, and S.-W. Cheong, Phys. Rev. Lett. **98**, 057601 (2007).
[15] Y. Naito, K. Sato, Y. Yasui, Y. Kobayashi, and M. Sato, J. Phys. Soc. Jpn. **76**, 023708 (2007).
[16] M. Enderle, B. Fåk, H.-J. Mikeska, R. K. Kremer, A. Prokofiev, and W. Assmuß, Phys. Rev. Lett. **104**, 237207 (2010).
[17] H. J. Koo, C. Lee, M.-H. Whangbo, G. J. McIntyre, and R. K. Kremer, Inorg. Chem. **50**, 2582 (2011).

[18]S.-L. Drechsler, S. Nishimoto, R. O. Kuzian, J. Málek, W. E. A. Lorenz, J. Richter, J. van den Brink, M. Schmitt, and H. Rosner, Phys. Rev. Lett. **106**, 219701 (2011).

[19]M. Mourigal, M. Enderle, R. K. Kremer, J. M. Law, and B. Fåk, Phys. Rev. B **83**, 100409(R) (2011).

[20]M. G. Banks, R. K. Kremer, C. Hoch, A. Simon, B. Ouladdiaf, J.-M. Broto, H. Rakoto, C. Lee, and M.-H. Whangbo, Phys. Rev. B **80**, 024404 (2009).

[21]S. Seki, T. Kurumaji, S. Ishiwata, H. Matsui, H. Murakawa, Y. Tokunaga, Y. Kaneko, T. Hasegawa, and Y. Tokura, Phys. Rev **82**, 064424 (2010).

[22]O. Oeckler and A. Simon, Z. Kristallogr.: New Cryst. Struct. **215**, 13 (2000).

[23]C. G. Barraclough and C. F. Ng, Trans. Faraday Soc. **60**, 836 (1964).

[24]T. J. Bastow and H. J. Whitfield, J. Mol. Struct. **58**, 305 (1980).

[25]T. J. Bastow, H. J. Whitfield, and G. K. Bristow, Phys. Lett. A **84**, 266 (1981).

[26]L. Zhao, T.-L. Hung, C.-C. Li, Y.-Y. Chen, M.-K. Wu, R. K. Kremer, M. G. Banks, A. Simon, M.-H. Whangbo, C. Lee, J. S. Kim, I. Kim, and K. H. Kim, Adv. Mater. **24**, 2469 (2012).

[27]M.-H. Whangbo, H.-J. Koo, and D. Dai, J. Solid State Chem. **176**, 417 (2003).

[28]P. E. Blöchl, Phys. Rev. B **50**, 17953 (1994).

[29]G. Kresse and D. Joubert, Phys. Rev. B **59**, 1758 (1999).

[30]G. Kresse and J. Furthmüller, Phys. Rev. B **54**, 11169 (1996).

[31]J. P. Perdew, K. Burke, and M. Ernzerhof, Phys. Rev. Lett. **77**, 3865 (1996).

[32]S. L. Dudarev, G. A. Botton, S. Y. Savrasov, C. J. Humphreys, and A. P. Sutton, Phys. Rev. B **57**, 1505 (1998).

[33]A. I. Liechtenstein, V. I. Anisimov, and J. Zaanen, Phys. Rev. B **52**, R5467 (1995).

[34]E. Bousquet and N. Spaldin, Phys. Rev. B **82**, 220402 (2010).

[35]D. Dai and M.-H. Whangbo, J. Chem. Phys. **114**, 2887 (2001).

[36]R. Zinke, S.-L. Drechsler, and J. Richter, Phys. Rev. B **79**, 094425 (2009).

[37]A. A. Tsirlin, R. Zinke, J. Richter, and H. Rosner, Phys. Rev. B **83**, 104415 (2011).

[38]*Handbook of Preparative Chemistry*, edited by G. Brauer (Academic, New York, 1963).

[39]R. L. Carlin, *Magnetochemistry* (Springer, Berlin, 1986).

[40]F. Heidrich-Meisner, A. Honecker, and T. Vekua, Phys. Rev. B **74**, 020403(R) (2006).

[41]For detailed numerical tables see [http://www.theorie.physik.uni-goettingen.de/∼honecker/j1j2-td/].

[42]D. Dai and M.-H. Whangbo, J. Chem. Phys. **114**, 2887 (2001); D. Dai, M.-H. Whangbo, H.-J. Koo, X. Rocquefelte, S. Jobic, and A. Villesuzanne, Inorg. Chem. **44**, 2407 (2005); H. J. Xiang, C. Lee, and M.-H. Whangbo, Phys. Rev. B **76**, 220411(R) (2007).

[43][http://www.ill.eu/d20/home/].

[44]For more details see the website of the FULLPROF program suite, [http://www.ill.eu/sites/fullprof/].

[45]L. Capogna, M. Reehuis, A. Maljuk, R. K. Kremer, B. Ouladdiaf, M. Jansen, and B. Keimer, Phys. Rev. B **82**, 014407 (2010).